Nucl. Part. Phys. Proc. xxx (xxxx) xxx

Contents lists available at ScienceDirect

Nuclear and Particle Physics Proceedings

journal homepage: www.elsevier.com/locate/nppp

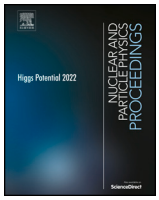

The inclusion of theory errors in PDF fits ☆

Andrea Barontini [a,b,*] on behalf of the NNPDF collaboration

[a] University of Milan, Italy
[b] INFN Milan, Italy

ARTICLE INFO

Keywords:
Parton distribution functions
MHOU
Theory errors
NNPDF

ABSTRACT

We present ongoing work towards incorporating the missing higher-order uncertainty (MHOU) determined through scale variations in the assessment of parton distribution functions (PDFs). Our PDFs fitting employs the NNPDF4.0 methodology and our theory covariance matrix framework to account for theory errors. This approach relies on the integration of MHOUs and their correlations via a theory covariance matrix. We validate our estimation and assess the impact of theory errors on the PDFs and on LHC phenomenology.

1. Introduction

The uncertainty of Parton Distribution Functions (PDFs) is a significant limitation for achieving precision physics at the LHC. The NNPDF4.0 [1] determination has attained a nominal accuracy at the percent level, due to methodological advancements and an augmented quantity of experimental data. It is imperative to evaluate the reliability of this precision and determine if the corresponding accuracy is consistent.

Referring to previous work, several papers have evaluated the impact of methodology on PDF uncertainties (see Refs. [2,3]). However, theoretical uncertainties that affect the QCD predictions used in PDF fit have yet to be included in such determinations (an exception being [4], whose objective however is slightly different from our own).

Theoretical uncertainties stem from several sources, including parametric factors (such as the values of heavy quark masses) and non-parametric factors. Nonetheless, the principal cause of theoretical uncertainties relates to missing higher orders in QCD computations (MHOUs). The current level of precision achieved in QCD calculations is typically at next-to-next-to-leading order (NNLO), with N^3LO corrections known only in limited cases [5]. At this perturbative level, the theoretical errors introduced by the missing higher-order terms are usually of the order of a few percent or larger, which is often comparable to the experimental systematics. For this reason, there is no justification for including the latter and not the former in the figure of merit used for PDF determination [2].

In Refs. [6,7], we have introduced the theory covariance matrix framework. This framework permits the systematic inclusion of theory uncertainties in PDF fits. Additionally, in these references, we presented the first instance of this methodology being applied to the construction of a set of NLO PDFs with theoretical uncertainties, based on the NNPDF3.1 [8] PDF set and methodology. Nevertheless, a complete global NNLO PDF set including MHOUs is not currently available.

The aim of this work is to introduce the updated versions of the global PDF determination of NNPDF4.0, that will be presented in the upcoming NNPDF4.0MHOU publication. This update will include more precise central values and uncertainties which now consider the incorporation of MHOUs in the PDF determination process. These PDFs will be the new default for NNPDF sets of parton distributions.

This manuscript is organised as follows. The first paragraph provides a comprehensive introduction to the concept of scale variations, along with the explicit equations utilized for estimation. Subsequently, we outline the theory covariance matrix methodology and the decisions made regarding prescription. Then, we detail the dataset used in this PDF determination, which is based on the NNPDF4.0 dataset. Also, we show the theory covariance matrices determined for this dataset and we benchmark them at NLO where they can be compared to the known NNLO results. Finally, we present our findings and assess the impact of

☆ Mini-Review talk presented at QCD23 - 38 years later, 23th International Conference in QCD (10-14/07/2023, Montpellier - FR).

* Correspondence to: University of Milan, Italy.
E-mail address: andrea.barontini@mi.infn.it (A. Barontini).

https://doi.org/10.1016/j.nuclphysbps.2023.11.002
Received 15 September 2023; Accepted 1 November 2023
Available online 8 November 2023

theoretical errors on our determination of PDFs. Additionally, we provide examples of using these PDFs in computing LHC processes, both to evaluate the impact of MHOUs on physical predictions and to demonstrate their practical applications.

2. Scale variations

We calculate MHOUs by supplementing the theory predictions with a theory covariance matrix obtained through scale variation. This paragraph presents a concise outline of its implementation in the NNPDF theory pipeline [9], particularly in the EKO [10] software.

3. Perturbative expansion and factorization

To establish the notation, we explicitly write out the perturbative expansion of an observable that is factorized in terms of a hard cross-section and PDFs. We are limiting our analysis to inclusive electroproduction using a single parton species for simplicity. We examine a structure function, $F(Q^2)$, which is dependent on a physical scale Q^2 and expressed through coefficient functions, $C(Q^2)$, expressed as an expansion in the strong coupling

$$a_s \equiv \frac{\alpha_s}{4\pi}, \tag{1}$$

and a PDF $f(Q^2)$. In Mellin space we simply have

$$F(Q^2) = C(Q^2) f(Q^2). \tag{2}$$

The partonic coefficient function at N^{k}LO it is given by

$$C\left(a_s(Q^2)\right) = a_s^m(Q^2) \sum_{j=0}^{k} \left(a_s(Q^2)\right)^j C_j \tag{3}$$

when the LO structure function is $O(a_s^m)$.

The scale dependence of the strong coupling $a_s(Q^2)$ and PDF $f(Q^2)$ are given by

$$\mu^2 \frac{a_s(\mu^2)}{\mu^2} = \beta(a_s(\mu^2)) = -\sum_{j=0}^{k} \left(a_s(\mu^2)\right)^{2+j} \beta_j, \tag{4}$$

$$\mu^2 \frac{f(\mu^2)}{\mu^2} = -\gamma\left(a_s(\mu^2)\right) f(\mu^2). \tag{5}$$

At N^{k}LO the beta function and anomalous dimensions are respectively given by

$$\beta(a_s(\mu^2)) = -\sum_{j=0}^{k} \left(a_s(\mu^2)\right)^{2+j} \beta_j, \tag{6}$$

$$\gamma\left(a_s(\mu^2)\right) = \sum_{j=0}^{k} \left(a_s(\mu^2)\right)^{1+j} \gamma_j, \tag{7}$$

where the coefficients β_j are known up to $k = 4$, while the coefficients γ_j are known exactly up to $k = 2$ and approximately for $k = 3$.

The solution to (5) can be written in form of an evolution kernel operator (EKO) $E(\mu^2 \leftarrow \mu_0^2)$ [10]

$$f(\mu^2) = E(\mu^2 \leftarrow \mu_0^2) f(\mu_0^2) \tag{8}$$

Including the anomalous dimension to N^{k}LO accuracy yields a PDF $f(Q^2)$ whose scale dependence has a resummed (next-to-)^k-leading-logarithmic (N^{k}LL) accuracy.

4. MHOU from scale variation

Predictions at the hadronic level rely on two quantities computed perturbatively: the coefficient functions (or partonic cross-sections), as shown in Eq. (3), and the anomalous dimensions, as shown in Eq. (7), which determine the scale dependence (Eq. (8)) of the PDFs. The prediction's uncertainty on either is caused by truncating the expansions which are expressed as a series in the strong coupling $a_s(Q^2)$, further expressed perturbatively by solving Eq. (4) in terms of a reference value, typically $a_s(M_Z)$.

The estimation of these MHOUs from scale variation is achieved by generating different expressions to a given accuracy, that differs by the subleading terms generated by the evaluation of the strong coupling at different scales. Starting with the coefficient function Eq. (3), we construct a scale-varied N^{k}LO coefficient function

$$\bar{C}(a_s(\mu^2), \rho_r) = a_s^m(\mu^2) \sum_{j=0}^{k} \left(a_s(\mu^2)\right)^j \bar{C}_j(\rho_r) \tag{9}$$

by requiring that

$$\bar{C}(a_s(\rho_r Q^2), \rho_r) = C(a_s(Q^2)) \left[1 + O(a_s)\right], \tag{10}$$

which fixes the coefficients $\bar{C}_j(\rho_r)$ in terms of C_j. Their explicit expressions up to NNLO are

$$\bar{C}_0(\rho) = C_0, \tag{11}$$

$$\bar{C}_1(\rho) = C_1 + m C_0 \beta_0 \ln \rho, \tag{12}$$

$$\bar{C}_2(\rho) = C_2 + \frac{m(m+1)}{2} C_0 \left(\beta_0\right)^2 \ln^2 \rho + \left((m+1) C_1 \beta_0 + m C_0 \beta_1\right) \ln \rho. \tag{13}$$

As can be seen in (11), at any given order C and $\bar{C}$ differ by subleading terms, so their difference can be taken as an estimate of the missing higher orders. We refer to this estimate of the MHOU on the partonic cross-sections as *renormalization* scale variation.

Through the same procedure, we obtain an estimate of the MHOU on the anomalous dimension: we construct a scale-varied N^{k}LO anomalous dimension

$$\bar{\gamma}(a_s(\mu^2), \rho_f) = a_s(\mu^2) \sum_{j=0}^{k} \left(a_s(\mu^2)\right)^j \bar{\gamma}_j(\rho_f) \tag{14}$$

by requiring that

$$\bar{\gamma}(a_s(\rho_f Q^2), \rho_f) = \gamma(a_s(Q^2)) \left[1 + O(a_s)\right], \tag{15}$$

which fixes the coefficients $\bar{\gamma}_j(\rho_f)$ in terms of γ_j. The corresponding expressions are the same as equation (11) in the particular case $m = 1$. Note that the uncertainty estimated through $\bar{\gamma}_j(\rho_f)$ translates into a MHOU on the PDF $f(Q^2)$ when this is expressed through Eq. (8) in terms of the PDFs at the parametrization scale. We refer to this estimate of the MHOU on the PDF as *factorization* scale variation.

By substituting the scale-varied anomalous dimension $\bar{\gamma}(\alpha(\mu^2), \rho_f)$ in the expression Eq. (8) of the PDF one can see [7] that factorization scale variation can be equivalently performed directly at the level of the PDF, by defining a scale-varied PDF $\bar{f}(Q^2, \rho_f)$ whose scale dependence is given by a scale-varied EKO $\bar{E}(Q^2 \leftarrow \mu_0^2, \rho_f)$:

$$\bar{f}(Q^2, \rho_f) = \bar{E}(Q^2 \leftarrow \mu_0^2, \rho_f) f(\mu_0^2), \tag{16}$$

and the scale-varied EKO $\bar{E}$, computed at N^{k}LL, differs by subleading terms from the original EKO:

$$\bar{E}(Q^2 \leftarrow \mu_0^2, \rho_f) = E(Q^2 \leftarrow \mu_0^2) \left[1 + O(a_s)\right]. \tag{17}$$

The scale-varied EKO can be constructed as

$$\bar{E}(Q^2 \leftarrow \mu_0^2, \rho_f) = K\left(a_s(\rho_f Q^2), \rho_f\right) E(\rho_f Q^2 \leftarrow \mu_0^2), \tag{18}$$

where at N^{k}LL (i.e. with the anomalous dimension computed at N^{k}LO) the extra evolution kernel $K(a_s(\rho_f Q^2), \rho_f)$ is given by the expansion

$$K\left(a_s(\rho_f Q^2), \rho_f\right) = \sum_{j=0}^{k} \left(a_s(\rho_f Q^2)\right)^j K_j(\rho_f). \tag{19}$$

Substituting this expansion in Eq. (17) fixes all coefficients $K_j(\rho_f)$ in terms of γ_j. Their explicit expressions up to NNLO are

$$K_0(\rho) = 1\,, \tag{20}$$

$$K_1(\rho) = \gamma_0 \ln \rho\,, \tag{21}$$

$$K_2(\rho) = \frac{1}{2}\gamma_0\left(\beta_0 + \gamma_0\right)\ln^2\rho + \gamma_1 \ln\rho\,. \tag{22}$$

Performing factorization scale variation at the level of the PDF is equivalent to the earlier approach at the level of the anomalous dimension.

Specifically, these two methods coincide up to sub-subleading terms. Within a PDF determination context, carrying out factorization scale variations at the level of the PDFs is simple, as it solely necessitates modifying the EKO utilised for computing PDF evolution. We use this method to conduct factorisation scale variation for the purpose of computing the theory covariance matrix.

5. The theory covariance matrix framework

The partonic cross-sections' and the PDFs' MHOUs are estimated through renormalization and factorization scale variations, respectively. They are incorporated into a theory covariance matrix, which is constructed as outlined in references [6,7]. Here we provide a brief summary on the construction recipe.

First, we define the shift in theory prediction for the i-th datapoint due to renormalization and factorization scale variation

$$\Delta_i(\rho_f, \rho_r) \equiv T_i(\rho_f, \rho_r) - T_i(0,0), \tag{23}$$

where $T_i(\rho_f, \rho_r)$ is the prediction for the i-th datapoint obtained by varying the renormalization and factorization scale by a factor ρ_r, ρ_f respectively.

Next, we choose a correlation pattern for scale variation, as follows [6,7]:

- factorization scale variation is correlated for all datapoints, because the scale dependence of PDFs is universal;
- renormalisation scale variation is correlated for all data points within the same category, so either belonging to the same observable (such as fully inclusive DIS cross-paragraphs) or different observables within the same process (such as, for example, the Z transverse momentum and rapidity distributions).

This necessitates the classification of processes; for example, we treat charged-current and neutral-current deep-inelastic scattering as distinct processes. The adopted process categorization is given in a later paragraph.

We finally define the theory covariance matrix between two datapoints i, j as

$$S_{ij} = n_m \sum_{V_m} \Delta_i(\rho_f, \rho_{r_i})\Delta_j(\rho_f, \rho_{r_j}), \tag{24}$$

where the sum runs over the space V_m of the m scale variations that are included and n_m is a normalization factor. The factorization scale ρ_f is always varied in a correlated way, while the renormalization scales ρ_{r_i}, ρ_{r_j} are varied in a correlated way ($\rho_{r_i} = \rho_{r_j}$) if datapoints i and j belong to the same category, but are varied independently if i and j belong to different categories. The normalization factors were computed for various choices of the space V_m of scale variations and for various values of m in Ref. [7], to which we refer for details.

As in Refs. [6,7] we consider scale variation by a factor 2, so

$$\kappa_f = \ln\rho_f = \pm\ln 4 \qquad \kappa_r = \ln\rho_r = \pm\ln 4. \tag{25}$$

In Ref. [7], the authors explored various options for the allowed parameter space.

One of these options involved allowing κ_r and κ_f to take on all values $(0, \pm\ln 4)$ for each datapoint, resulting in a 9-point prescription with $m = 8$ variations from the central value.

Here we adopt as a default the commonly used 7-point prescription, with $m = 6$, which is obtained from the former by discarding the two outermost variations, in which $\kappa_r = +\ln 4$, $\kappa_f = -\ln 4$ or $\kappa_r = -\ln 4$, $\kappa_f = +\ln 4$. The explicit expressions for the theory covariance matrix with the 7-point prescription are given in Eqs. (4.18)-(4.19) of Ref. [7].

6. Dataset and validation

In this paragraph, we begin by specifying the datasets and process categorisation utilized for determining the theory covariance matrix and for the fit. We then present the theory covariance matrices for both NLO and NNLO. Finally, we concisely describe and employ the validation procedure previously utilised in [6,7].

7. Dataset definition and process categorization

For the PDF set with MHOUs included, we utilized the entire NNPDF4.0 dataset, which is described in detail in [1]. To ensure the accuracy of the scale variation method, however, different kinematic cuts were applied to the data, similarly to what was carried out in [6].

For the NNLO fit, we utilized identical DIS cuts to those presented in [6]. This corresponded to a value of $Q^2 = 13.9$ GeV^2. Additionally, we introduced a lower maximum accepted value for $\tau = M^2/s$ for the fixed-target DY data. Specifically, Max(τ) was reduced to 0.02 from its previous value of 0.08. Both cuts are motivated by the scale variations method to guarantee that the energy scale used to evaluate the strong coupling, such as $\kappa^2_{r/f}Q^2$ in DIS, remains perturbative when $\kappa^2_{r/f} = (0.5)^2$. The NNLO fit consists of a total of 3521 points.

The cuts for the NLO case are largely the same. However, scale variations in NLO for DIS are known to be unreliable and unstable for $Q^2 \lesssim 18$ GeV^2. Therefore, we have chosen to use a higher cut, specifically $Q^2 = 18$ GeV^2, for the NLO DIS predictions. As a result, the total number of points for determining the NLO PDFs is 3278.

As detailed previously, the theory covariance matrix is formulated to incorporate a correlation pattern for scale variations. Specifically, the renormalisation scale variation is correlated for all data points within the same category. This requires the data used for determining PDFs to be classified in various process categories. Note that this was also done in [6], but in this work we propose an improved categorization. Here we summarise our choices.

As in [6], we considered charged current and neutral current DIS as different processes. We did the same for charged current and neutral current DY, as opposed to the single DY process used in [6].

We kept the Jets and Top processes but we also added singletop, photon and dijet.

8. Theory covariance matrices at NLO and NNLO

The theory covariance matrices at NLO and NNLO are shown in Fig. 1. As expected, the absolute value of the NNLO theory covariance matrix is nearly one-tenth of the NLO theory covariance matrix. Nonetheless, the correlations between datasets appear to stay relatively consistent in shape. Additionally, it proves worthwhile to observe the influence of the theory covariance matrix once added to the experimental covariance matrix, as this sum is actually utilized in the fit. Fig. 2 displays the normalized sum of the experimental and theory covariance matrices for both NLO and NNLO. The off diagonal elements are expectedly higher at NLO than at NNLO where the effect of theory covariance matrix becomes almost negligible due to the dominant experimental contribution.

9. Comparing NLO theory errors to known NNLO shifts

To verify the accuracy of our theory error estimation, and whether it is able to reproduce the real difference between a given perturbative order and the next, we perform the same kind of validation proposed

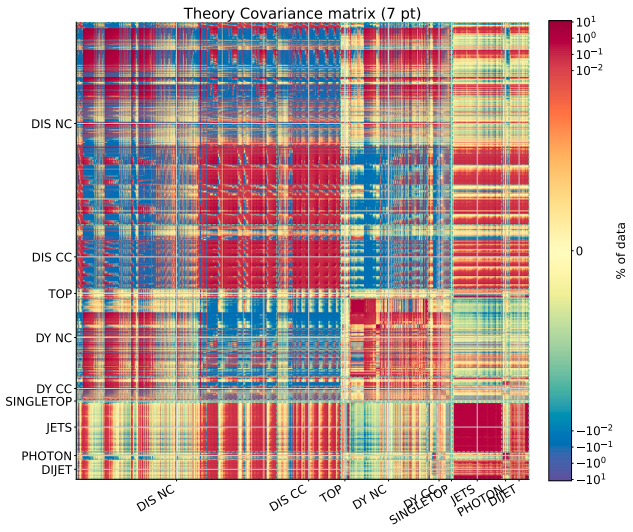

(a) NLO

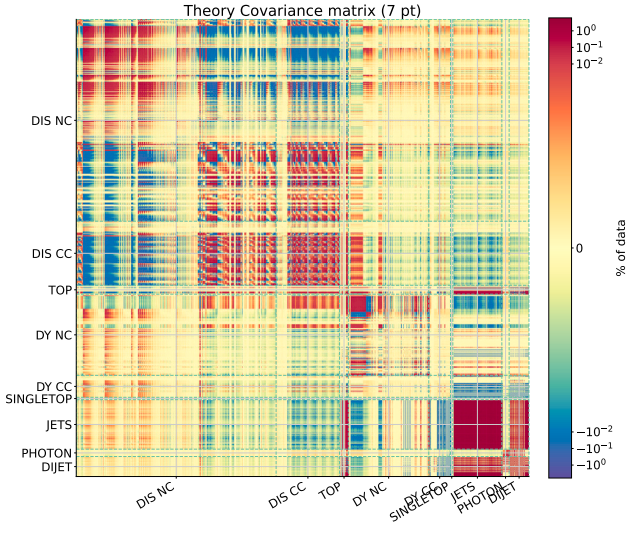

(b) NNLO

Fig. 1. Theory covariance matrix plots for NLO (top) and NNLO (bottom).

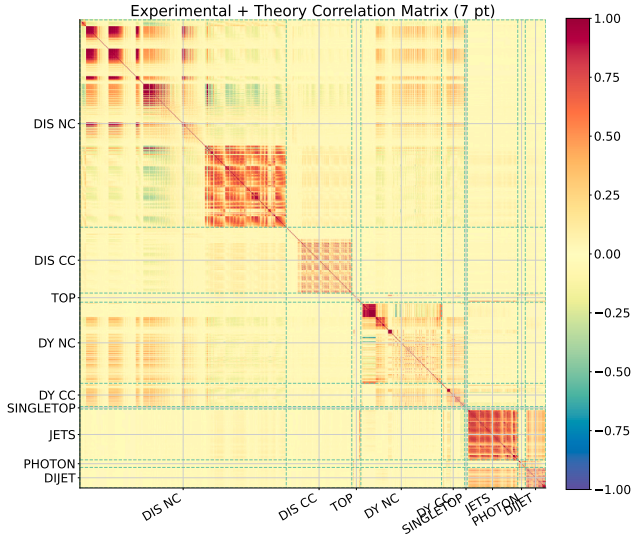

(a) NLO

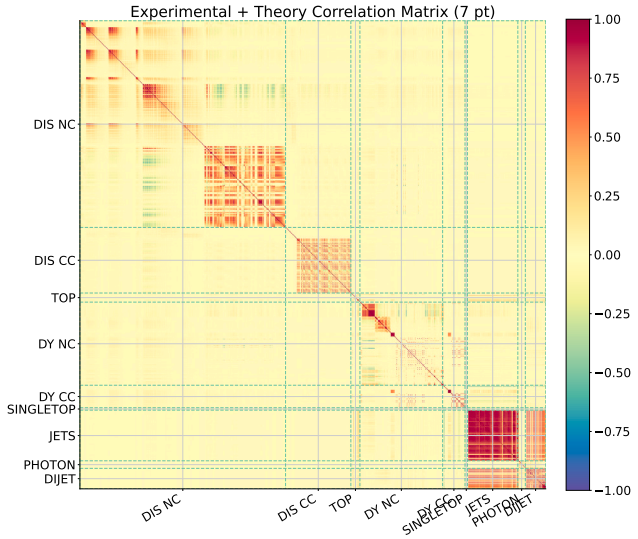

(b) NNLO

Fig. 2. Theory covariance matrix plus experimental covariance matrix normalized to diagonal element for NLO (top) and NNLO (bottom).

in [6,7]. This involves comparing the diagonal values of the theory covariance matrix at NLO, specifically S_{ii}^{NLO}, with the expected known difference between NNLO and NLO, specifically $T_i^{\mathrm{NNLO}}(0,0) - T_i^{\mathrm{NLO}}(0,0)$, for all data points described in the previous paragraph. This comparison is illustrated in Fig. 3 where both the differences and theoretical uncertainties are normalized with respect to the central NLO predictions $T_i^{\mathrm{NLO}}(0,0)$. The validation results indicate that our estimation of the theoretical uncertainties is somewhat conservative, particularly in the case of DIS, and that it effectively captures the behaviour of the NNLO.

10. Results

In this paragraph we summarise the main achievements of this work: the preliminary NLO and NNLO PDFs determinations that systematically accounts for theory errors. In particular, first we show the impact of including theory errors in a PDF fit, mainly focusing on how the PDF central values and the uncertainties change.

Then, we focus on the perturbativity of the results, comparing NLO and NNLO PDFs with and without theory errors.

Finally, we show the impact of these new PDF set on phenomenology, again focusing on the perturbativity of the result.

11. Impact of theory errors

In Fig. 4 we show the comparison of the gluon and singlet NNLO PDFs with and without theory errors. Although the theory covariance matrix introduces a source of uncertainties, the PDF uncertainties persist at about the same size even with the inclusion of theory errors, except in the case of the singlet at a relatively small x-value. Moreover, central values appear to be more susceptible to the influence of theory errors than uncertainties. This outcome is unsurprising given the deweighting effect of the theory covariance matrix on the datasets that are most affected by theory errors.

12. Perturbativity improvements

Including theory errors in a PDF fit is expected to significantly enhance perturbativity. Specifically, this entails that the NLO PDFs with theory errors will approximate the NNLO PDFs more closely than the NLO PDFs without theory errors. Fig. 5 shows a comparison of the ratios NNLO/NLO for gluon and singlet PDFs with and without accounting for theoretical errors. Overall, the NLO PDFs are closer to the NNLO

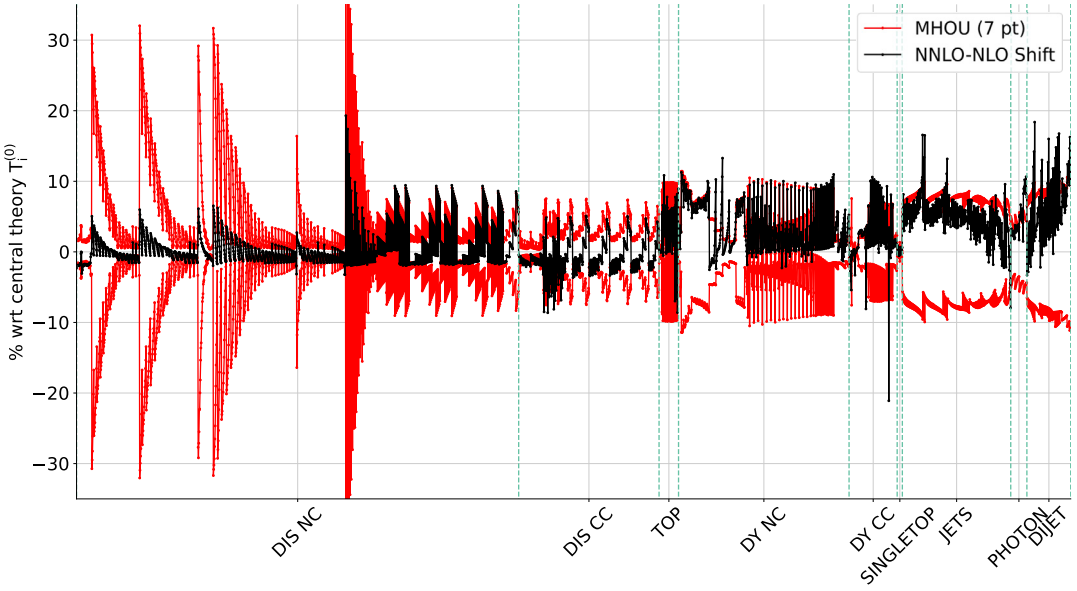

Fig. 3. Comparison of the difference between the NNLO and the NLO predictions (in black) to the theory errors as estimated by the diagonal entry of the theory covariance matrix S at NLO for all the datapoints.

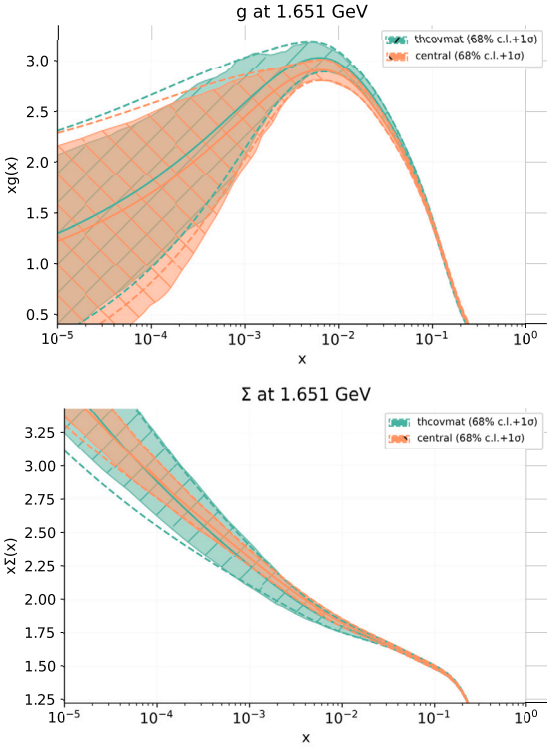

Fig. 4. The NNLO gluon and the singlet PDFs in logarithmic scale, as determined with (in green) and without (in orange) theory errors. (For interpretation of the colours in the figure(s), the reader is referred to the web version of this article.)

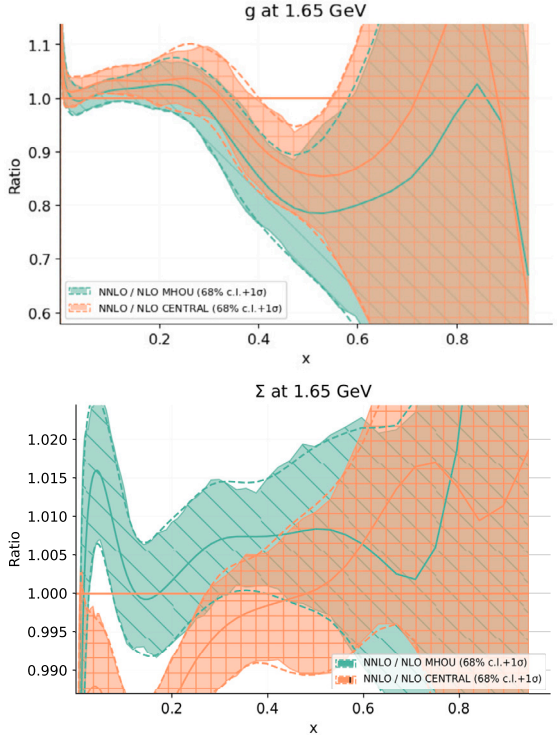

Fig. 5. NNLO/NLO gluon and singlet PDFs with (in green) and without (in orange) theory errors.

PDFs when considering theoretical errors, particularly for the singlet PDF around $x = 0.1$, as can be observed.

It is anticipated that using such PDFs to compute predictions will yield similar results, as demonstrated in the next paragraph.

13. Impact on phenomenology

Finally, we provide an example of how the inclusion of theory errors in the NNPDF4.0 PDFs influences relevant predictions for phenomenology. Specifically, Fig. 6 presents Higgs production computed via NLO and NNLO PDFs, with and without errors (produced with PineAPPL [11]). To simplify the comparison of PDFs, the matrix element used for such predictions has been kept fixed at NLO in all four cases. We confirm that accounting for theory errors improves perturbativity, also at the level of predictions.

14. Conclusions

In this work we summarised some of the results that will be presented in the upcoming NNPDF4.0MHOU publication. In particular, we

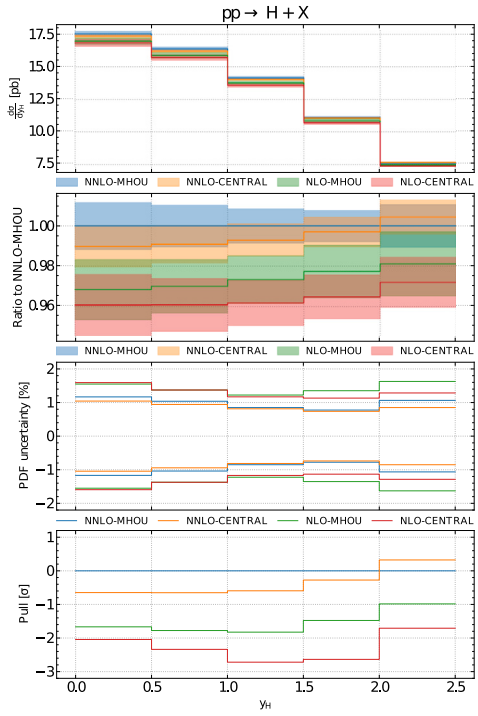

Fig. 6. Higgs production predictions obtained with NLO and NNLO PDFs with and without theory errors [11]. Note that the matrix element employed is always at NLO to facilitate the PDF comparison. It is relevant to note that the NLO-MHOU (in green) prediction is always closer to the NNLO (in blue or in orange) predictions than the NLO-CENTRAL (i.e. without theory errors) one (in red).

presented our ongoing work to produce the first NNLO PDF determination that systematically includes theory errors affecting the theoretical predictions entering in the fit. We stressed that accounting for the theory errors is necessary to get faithful central values and uncertainties as theory errors are now of about the same size of experimental and methodological errors. We have outlined how the scale variations technique can be utilised to estimate theory errors and introduced a general framework, i.e. the theory covariance matrix formalism, for incorporating such theory errors into a PDF fit. We validated our estimation by examining the NLO and NNLO theory covariance matrices, as well as comparing our NLO estimate to the known NNLO-NLO shifts. Lastly, we presented our final results, focusing on the improvements on the perturbativity of both the PDFs themselves and of the predictions obtained using PDFs that account for theory errors. Additionally, our findings indicated that incorporating the theory covariance contribution to the total covariance matrix employed in the fit does not notably impact the ultimate uncertainties of the PDFs. On the contrary, it affects their central values.

Declaration of competing interest

The authors declare that they have no known competing financial interests or personal relationships that could have appeared to influence the work reported in this paper.

Data availability

Data will be made available on request.

References

[1] R.D. Ball, et al., The path to proton structure at 1% accuracy, Eur. Phys. J. C 82 (5) (2022) 428, https://doi.org/10.1140/epjc/s10052-022-10328-7, arXiv:2109.02653.

[2] L. Del Debbio, T. Giani, M. Wilson, Bayesian approach to inverse problems: an application to NNPDF closure testing, Eur. Phys. J. C 82 (4) (2022) 330, https://doi.org/10.1140/epjc/s10052-022-10297-x, arXiv:2111.05787.

[3] R.D. Ball, J. Cruz-Martinez, L. Del Debbio, S. Forte, Z. Kassabov, E.R. Nocera, J. Rojo, R. Stegeman, M. Ubiali, Response to "Parton distributions need representative sampling", arXiv:2211.12961, 2022.

[4] J. McGowan, T. Cridge, L.A. Harland-Lang, R.S. Thorne, Approximate N^3LO parton distribution functions with theoretical uncertainties: MSHT20aN^3LO PDFs, Eur. Phys. J. C 83 (3) (2023) 185, https://doi.org/10.1140/epjc/s10052-023-11236-0 Erratum: Eur. Phys. J. C 83 (2023) 302, arXiv:2207.04739.

[5] J. Baglio, C. Duhr, B. Mistlberger, R. Szafron, Inclusive production cross sections at N^3LO, J. High Energy Phys. 12 (2022) 066, https://doi.org/10.1007/JHEP12(2022)066, arXiv:2209.06138.

[6] R. Abdul Khalek, et al., A first determination of parton distributions with theoretical uncertainties, Eur. Phys. J. C 79 (2019) 838, https://doi.org/10.1140/epjc/s10052-019-7364-5, arXiv:1905.04311.

[7] R. Abdul Khalek, et al., Parton distributions with theory uncertainties: general formalism and first phenomenological studies, Eur. Phys. J. C 79 (11) (2019) 931, https://doi.org/10.1140/epjc/s10052-019-7401-4, arXiv:1906.10698.

[8] R.D. Ball, et al., Parton distributions from high-precision collider data, Eur. Phys. J. C 77 (10) (2017) 663, https://doi.org/10.1140/epjc/s10052-017-5199-5, arXiv:1706.00428.

[9] A. Barontini, A. Candido, J.M. Cruz-Martinez, F. Hekhorn, C. Schwan, Pineline: industrialization of high-energy theory predictions, arXiv:2302.12124, 2023.

[10] A. Candido, F. Hekhorn, G. Magni, EKO: evolution kernel operators, Eur. Phys. J. C 82 (10) (2022) 976, https://doi.org/10.1140/epjc/s10052-022-10878-w, arXiv:2202.02338.

[11] S. Carrazza, E.R. Nocera, C. Schwan, M. Zaro, PineAPPL: combining EW and QCD corrections for fast evaluation of LHC processes, J. High Energy Phys. 12 (2020) 108, https://doi.org/10.1007/JHEP12(2020)108, arXiv:2008.12789.